Biophysical Journal, Volume *111*

Supplemental Information

Nanonet Force Microscopy for Measuring Cell Forces

Kevin Sheets, Ji Wang, Wei Zhao, Rakesh Kapania, and Amrinder S. Nain

Supporting Material

Derivation of Force Equation

Equations used to calculate forces based on fiber deflection are derived from Timoshenko's tie rod with lateral loading. After deriving equations for a beam under compressive load '*S*', a negative sign is included to convert to a beam under tension. A summary/excerpt of the relevant derivation from Timoshenko's "Strength of Materials" book is provided below(1).

Assuming a hinged tie rod is held under compression and loaded perpendicularly to the fiber axis with a vertical single point load, *P*, the differential equations describing the deflection curve up to the location of the point load, c, and following the point load are:

$$EI\frac{d^2y}{dx^2} = -Sy - \frac{Pc}{l}x \quad \text{(a)}$$

$$EI\frac{d^2y}{dx^2} = -Sy - \frac{P(l-c)}{l}(l-x) \quad \text{(b)}$$

We then define:

$$\frac{S}{EI} = \lambda^2$$

The solutions to (a) and (b) are then:

$$y = C_1 cos\lambda x + C_2 sin\lambda x - \frac{Pc}{Sl}x \quad \text{(c)}$$

$$y = C_3 cos\lambda x + C_4 sin\lambda x - \frac{P(l-c)}{Sl}(l-x) \quad \text{(d)}$$

Boundary conditions are then applied considering there are no fiber deflections at the pinned ends of the strut:

From the bounday condition we know

In the Eq. (c), x=0, y=0, we have,

$$C_1 = 0$$

In the Eq.(d), x=l, y=0, we have,

$$C_3 = -C_4 tan\lambda l$$

The other two integration constants are achieved by recognizing deflection and slope continuity at the point of load application:$x = l - c,\ y_1 = y_2;\ d\,y_1/d\,x = d\,y_2/d\,x$. From Eqs.(c) and (d), we have

$$\lambda(l-c)$$
$$sin\lambda(l-c) - tanplcos$$

$$\lambda(l-c) = C_4$$
$$C_2 sin$$

$$\lambda(l-c)$$
$$cos\lambda(l-c) + tan\lambda lsin$$

$$\lambda(l-c) = C_4\lambda$$
$$C_2\lambda cos$$

From which

$$C_2 = \frac{P}{S}\frac{sin\lambda c}{\lambda sin\lambda l}$$

$$C_4 = \frac{-P}{S}\frac{sin\lambda(l-c)}{\lambda tan\lambda l}$$

Substituting the integration constants into (c) gives the equation for fiber position as a result of compressive loading, we obtain the deflection profile,

$$y = \begin{cases} \dfrac{Psin\lambda c}{S\lambda sin\lambda l} sin\lambda x - \dfrac{Pc}{Sl}x (0 \le x \le l-c) \\ \dfrac{Psin\lambda(l-c)}{S\lambda sin\lambda l} sin\lambda(l-x) - \dfrac{P(l-c)}{Sl}(l-x) (l-c \le x \le l) \end{cases}$$

The above equation can easily be modified to describe a fiber under tension by changing the sign of S. Doing so changes λ^2 to $-\lambda^2$ as well, making$\lambda\sqrt{-1} = \lambda i$. Therefore, by substituting $-S$ and λi in place of S and λ in the formulas obtained earlier, the formula for a beam under tension may be obtained. Recalling that:

$$sin\lambda i = isinh\lambda, \quad cos\lambda i = coshp\lambda, \quad tan\lambda i = tanh\lambda$$

The left-hand side $(0 \le x \le l-c)$ of the tie rod can be solved for:

$$y = \frac{-Psinh\lambda c}{S\lambda sinh\lambda l} sinh\lambda x + \frac{Pc}{Sl}x$$

And the right-hand side $(l-c \le x \le l)$:

$$y = \frac{-Psinh\lambda(l-c)}{S\lambda sinh\lambda l} sinh\lambda(l-x) + \frac{P(l-c)}{Sl}(l-x)$$

Having defined the deflection profile under a single point load, the two points load formula (as used to calculate forces on nanonets) may be obtained by superimposing a second load. The deflections at points a and b, δ_a and δ_b, respectively, are (P_b is at the left side of P_a)

$$\delta_a = \left(\frac{-P_a sinh[\lambda(L-a)]}{S\lambda sinh[\lambda L]} sinh[\lambda a] + \frac{P_a(L-a)}{SL}a\right) - \frac{P_b sinh[\lambda(L-b)]}{S\lambda sinh[\lambda L]} sinh[\lambda a] + \frac{P_b(L-b)}{SL}a$$

$$\delta_b = \frac{-P_a sinh[\lambda a]}{S\lambda sinh[\lambda L]} sinh[\lambda(L-b)] + \frac{P_a(L-b)}{SL}a + \left(\frac{-P_b sinh[\lambda(L-b)]}{S\lambda sinh[\lambda L]} sinh[\lambda b] + \frac{P_b(L-b)}{SL}b\right)$$

where L, a and b are the length of the rod, position of load P_a and poistion of load P_b measured from the right end. The minus sign represents the deflection downward.

AFM Characterization of Fiber Structural Stiffness

Fibers must have structural stiffnesses that are soft enough to permit appreciable deformation under single cell-scale loads that can be accurately measured optically while simultaneously remaining stiff enough to prevent plastic deformations (approximately <5% of the span length) (2, 3). To quantify stiffness, atomic force microscopy (AFM) was used in tapping mode with tipless cantilevers. As the cantilever presses on a single fiber, the cantilever and fiber deflection are recorded and converted to a stiffness value. Parametric evaluation of fiber properties on structural stiffness and associated modeling showed fiber structural stiffnesses acceptably ranged from ~5-20 nN/µm at the center of the fibers. Due to the competing contributions of fiber length and diameter, it is possible to arrive at the same structural stiffness with a short, thin diameter fiber and a long, large diameter fiber, as shown by the overlapping red and blue lines in Fig. S1A. A heat map plot generated in MATLAB further demonstrates how structural stiffness changes as a function of both fiber length and fiber diameter within the nanonet design space (Fig. S1B). Residual stress measurements achieved through AFM-based fiber breakage show that each fiber, independent of fiber diameter, carries 4.1 MPa residual stress as a result of the STEP spinning process. Therefore, the typically-used fiber diameter of 400 nm is assigned a constant pre-tension value of 0.54 µN, and this value increases for larger diameter fibers.

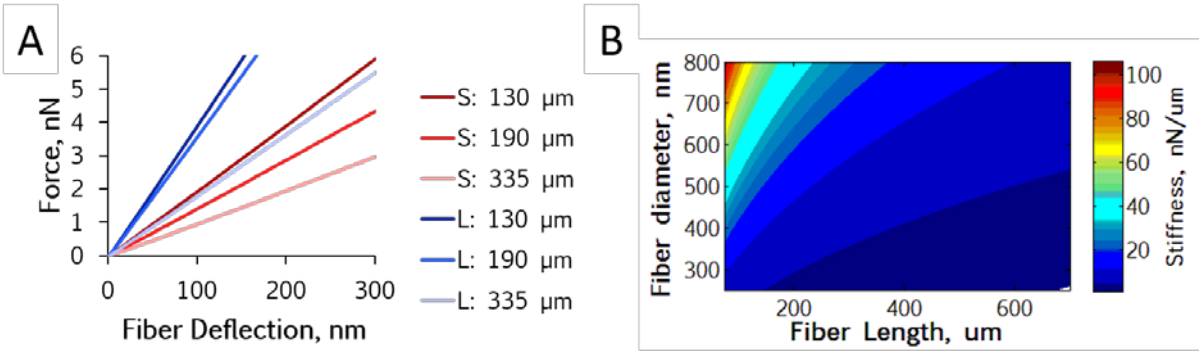

FIGURE S1 (*A*) The slope of the AFM force-deflection curves are converted to stiffness values. The effect of fiber diameter (S: small (~250 nm, red), L: large (~500 nm, blue)) as well as fiber length (dark shading: ~130 µm, medium shading: ~190 µm, and light shading: ~335 µm) are seen by differences in slope. (*B*) Mathematical modeled iso-stiffness lines demonstrate how a short, small diameter fiber can have the same stiffness as a long, large diameter fiber (plot generated from MATLAB code of governing equations shown above).

Viscoelastic Strain Rate Phenomena

The first test to determine the extent of cellular viscoelasticity on STEP fibers was to perform a phase evaluation at various strain rates. Cells were cyclically stretched and both fiber and probe displacement were tracked for strain rates ranging from 1-30 µm/s. Plotting the displacements together reveals that viscoelastic effects appear at low strain rates and diminish at high rates (Fig. S2). The probe and passive fiber are in-phase during active pull (positive slope). Probe lag, as demonstrated by the solid lines following after the dashed lines, is observed when the probe returns to zero deflection (negative slope) for low strain rate cases. This is indicative of viscoelastic behavior: a purely elastic interaction would yield in-phase displacements throughout testing, yet instead an out-of-phase phenomenon is observed during relaxation. This behavior may originate either from the cell losing elasticity (becoming softer) when the active component is removed during relaxation, or from the release of tension built up in the fiber during active pull. In either case, probe lag effects are significantly diminished upon reaching the 3-5 µm/s strain rate threshold, and are not visible at rates higher than those (Figure S2 *B*). This suggests that cells pulled near the threshold strain rate should behave

'purely elastically' on STEP fibers, and any strain rate effects would plateau near these values.

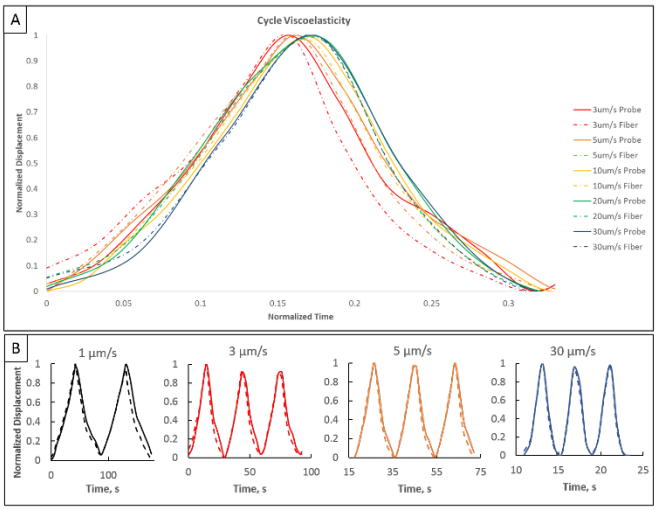

FIGURE S2 Cycle viscoelasticity as a function of strain rate. Data shows that probe lag effects are dramatic at low strain rates compared to high strain rates.

Stress Relaxation Tests

As cells experience forces, interactions between cytosol and cytoskeletal structures within their semi-permeable membrane elicit strain-rate dependent responses, but identifying physiological mechanisms for this behavior has proven difficult (4, 5). Since viscoelasticity can alter the measured force at different strain rates, it is nonetheless an important parameter to qualitatively describe even without complete knowledge of the contribution of individual cellular components (6). Viscoelastic response is quantified through the classic stress relaxation test (5, 7). In this approach, the cell undergoes an instantaneous step strain which is held constant while the cell relaxes. By tracking the rate at which this relaxation occurs, data can be fitted into viscoelastic models to establish baseline expected mechanical performance. Here, we use the standard linear solid (SLS) model which is composed of a spring (k_1) in parallel with a spring and damper that are in series (k_2 and η). When a step strain is applied, the force relaxation is described by: (8)

$$F = \left(\frac{F_0}{k_1+k_2}\right) k_2 + k_1 e^{\frac{-k_1 t}{\eta}} \qquad \text{(Eqn. S1)}$$

Where F_0 is the initial force observed upon instantaneous strain and t is time. The advantage of fitting data to such models is that one can distinguish rate-dependent mechanical response of the cell from rate-independent ones, yet difficulty has historically emanated from drawing biological significance from these three parameters (9, 10). Moreo et al used an SLS model to describe mechanosensory response to varying substrate stiffnesses (11). In this model, three cytoskeletal elements were assumed to play a significant role in cell mechanics: microtubules, actin, and acto-myosin contractions. From the concept of tensegrity, microtubules are assumed to be compressional elements with actin primarily the tensile element (12, 13). Therefore, microtubule-based disruptions would be rate-independent and suitable for the k_1 assignment. Likewise, since actin is bundled to the acto-myosin contraction and exhibits strain stiffening (9), it is assigned to k_2 since it is in series with the viscous component η. Lastly, pairing acto-myosin contraction with the cell viscosity parameter η may be an oversimplification but would capture viscous-like active cell adjustments to external forces (14).

Stress relaxation tests were performed by applying an instantaneous step displacement of 16 $\pm$ 6 µm at 100 µm/s and data was fitted to the SLS model (Fig. S3). Cells that

experience a step strain exhibit viscoelasticity and require several seconds to fully relax. Fig. S3 *B* shows elongation of the cell throughout the test. Figure S3 *C* shows that peak membrane velocities during these tests were found to be on the order of 1 µm/s, which may partially explain why the system exhibits probe lag near this strain rate. The three-element SLS model was used to fit relaxation data as shown by the dashed line in Fig. S3 E. Cells relaxed to 85 – 95% of their original force value, with the major contribution stemming from k_1 (shown in blue in Fig. S3E). The predicted assignment of microtubules, actin, and acto-myosin contractility to the three elements in the SLS model by Moreo et al. presents a testable case with the use of selective knockout agents. Microtubules were therefore depolymerized with 10 µM nocodazole administration (15). The acto-myosin contractile element of the cell was disrupted with 50 µM blebbistatin, which interferes with myosin-II (16). Lastly, actin can be depolymerized with cytochalasin D, but doing so would interfere with the acto-myosin component as well so this agent was not used (17). Normalized values for k_1, k_2, and η plotted in Figure S3 F show shifting in the relative contributions from k_2 to η for both drug cases, suggesting the correlation of these parameters to biological components is either an oversimplification or that the SLS model is unable to capture this dependency.

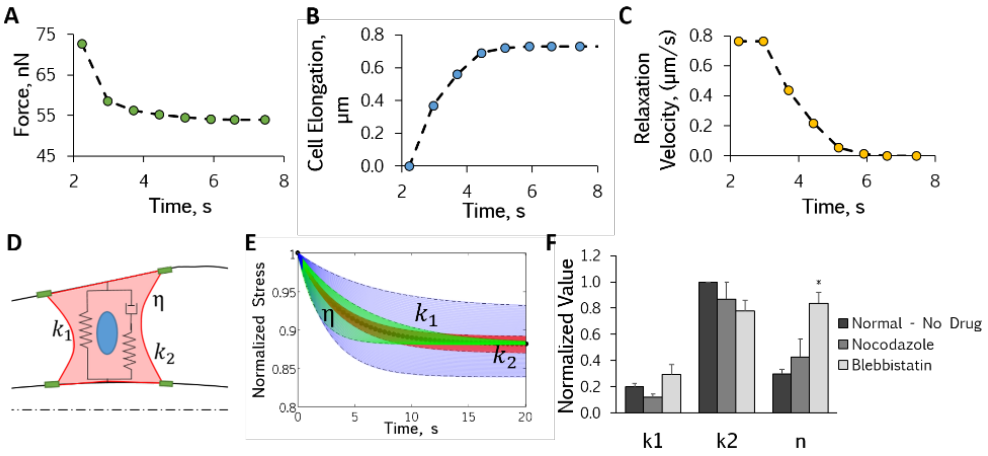

FIGURE S3 Stress relaxation test and associated SLS modeling. Representative single cell data for: A) Force reduction over time, B) cell elongation after step-strain is applied and held constant, and C) relaxation velocity during the test, D) Schematic of the 3-element SLS model, E) SLS parametric modeling showing dependence on k_1 (blue), k_2 (red), and η (green) with shaded regions representing standard deviation, F) Cytoskeleton knockdown drugs nocodazole (microtubules) and blebbistatin (myosin) cause shift in major contribution from k_2 to η (n = 25).

1. Timoshenko, S. 1983. Strength of Materials, Pt. 2: Advanced Theory and Problems, Part 2. R. E. Krieger Publishing Company.

2. Carlisle, C.R., C. Coulais, and M. Guthold. 2010. The mechanical stress–strain properties of single electrospun collagen type I nanofibers. Acta Biomater. 6: 2997–3003.

3. Gestos, A., P.G. Whitten, G.M. Spinks, and G.G. Wallace. 2013. Tensile testing of individual glassy, rubbery and hydrogel electrospun polymer nanofibres to high strain using the atomic force microscope. Polym. Test. 32: 655–664.

4. Janmey, P. a, S. Hvidt, J. Käs, D. Lerche, a Maggs, et al. 1994. The mechanical properties of actin gels. Elastic modulus and filament motions. J. Biol. Chem. 269:

32503–32513.

5. Darling, E.M., S. Zauscher, J. a Block, and F. Guilak. 2007. A thin-layer model for viscoelastic, stress-relaxation testing of cells using atomic force microscopy: do cell properties reflect metastatic potential? Biophys. J. 92: 1784–91.

6. Ketene, A.N., P.C. Roberts, A. a Shea, E.M. Schmelz, and M. Agah. 2012. Actin filaments play a primary role for structural integrity and viscoelastic response in cells. Integr. Biol. (Camb). : 540–549.

7. Nagayama, K., S. Yanagihara, and T. Matsumoto. 2007. A novel micro tensile tester with feed-back control for viscoelastic analysis of single isolated smooth muscle cells. Med. Eng. Phys. 29: 620–8.

8. Leipzig, N.D., and K. a K. a Athanasiou. 2005. Unconfined creep compression of chondrocytes. J. Biomech. 38: 77–85.

9. Wen, Q., and P.A. Janmey. 2011. Polymer physics of the cytoskeleton. Curr. Opin. Solid State Mater. Sci. 15: 177–182.

10. Mofrad, M.R.K. 2009. Rheology of the Cytoskeleton. Annu. Rev. Fluid Mech. 41: 433–453.

11. Moreo, P., J.M. García-Aznar, and M. Doblaré. 2008. Modeling mechanosensing and its effect on the migration and proliferation of adherent cells. Acta Biomater. 4: 613–21.

12. Ingber, D.E., S.R. Heidemann, P. Lamoureux, E. Robert, A.D. Bicek, et al. 2012. Opposing views on tensegrity as a structural framework. : 1663–1678.

13. Ingber, D.E., N. Wang, and D. Stamenović. 2014. Tensegrity, cellular biophysics, and the mechanics of living systems. Rep. Prog. Phys. 77: 046603.

14. Yoshinaga, N., and P. Marcq. 2012. Contraction of cross-linked actomyosin bundles. Phys. Biol. 9: 046004.

15. Ezratty, E.J., M.A. Partridge, and G.G. Gundersen. 2005. Microtubule-induced focal adhesion disassembly is mediated by dynamin and focal adhesion kinase. Nat Cell Biol. 7: 581–590.

16. Fournier, M.F., R. Sauser, D. Ambrosi, J.-J. Meister, and A.B. Verkhovsky. 2010. Force transmission in migrating cells. J. Cell Biol. 188: 287–97.

17. Schliwa, M. 1982. Action of Cytochalasin D on Cytoskeletal Networks High-voltage Electron Microscopy Cytochalasin D Applied to Intact Cells. J. Cell Biol. 92: 79–91.